Electronic Supporting Information

Platinum(II)-Gold(I) Heterotrinuclear Complexes with N,N'-Diarylamine-functionalized Acetylide Ligands for Red Electroluminescence

Hao Zeng,[a,c] Jin-Yun Wang,[a,*] Lin-Xi Shi,[a] Li-Yi Zhang,[a] and Zhong-Ning Chen[a,b,*]

[a] *State Key Laboratory of Structural Chemistry, Fujian Institute of Research on the Structure of Matter, Chinese Academy of Sciences, Fuzhou, Fujian 350002, China. E-mail: czn@fjirsm.ac.cn*

[b] *Fujian Science & Technology Innovation Laboratory for Optoelectronic Information of China, Fuzhou, Fujian 350108, China*

[c] *University of Chinese Academy of Sciences, Beijing, 100039, China*

Experimental Section

$Pt(PPh_3)_2(C{\equiv}C\text{-}TPA)_2$ (Pt-1). Under dry argon atmosphere, $Pt(PPh_3)_2Cl_2$ (0.4 mmol), 4-ethynyl-N,N'-diphenylaniline (1.0 mmol), CuI (1 mg) and Et_3N (1 mL) were dissolved in 40 mL $CHCl_3$ with stirring at 60℃ for 6 h. The reaction was monitored by thin layer chromatography (TLC). After completion of reaction, the solvent was removed under reduced pressure. The product was purified by silica gel column chromatography using CH_2Cl_2-petroleum (4:1, v/v) as eluent to give yellow powder. Yield: 53%. ^{1}H NMR (600 MHz, $CDCl_3$, ppm): 8.16-7.70 (m, 12H), 7.60-7.34 (m, 24H), 7.23-6.90 (m, 16H), 6.79-6.54 (m, 3H), 6.35-6.00 (m, 3H). ^{31}P NMR (243 MHz, $CDCl_3$, ppm): 19.3 (s, 1P, J_{Pt-P} = 2668 Hz).

$Pt(PPh_3)_2(C{\equiv}C$-N,N-diphenylthiophen-2-amine$)_2$ (Pt-2). This compound was prepared by the same stnthetic procedure as that of **Pt-1** except for the use of 5-ethynyl-N,N-diphenylthiophen-2-amine in place of 4-ethynyl-N,N'-diphenylaniline. Yield: 48%. ^{1}H NMR (400 MHz, $CDCl_3$, ppm): 7.77-7.70 (m, 12H), 7.40-7.32 (m, 18H), 7.23-7.16 (m, 8H), 7.07-6.92 (m, 12H), 6.21-6.05 (d, 2H, J = 4.0 Hz), 5.77-5.70 (d, 2H, J = 4.0 Hz). ^{31}P NMR (162 MHz, $CDCl_3$, ppm): 17.7 (s, 1P, J_{Pt-P} = 2625 Hz).

$Pt(PPh_3)_2(C{\equiv}C$-4-phenyl-4H-dithieno[3,2-b:2',3'-d]pyrrole$)_2$ (Pt-3). This compound was prepared by the same stnthetic procedure as that of **Pt-1** except for the use of 2-ethynyl-4-phenyl-4H-dithieno[3,2-b:2',3'-d]pyrrole in place of 4-ethynyl-N,N'-diphenylaniline. In addition, the product was purified by silica gel column chromatography using CH_2Cl_2-petroleum (2 : 1, v/v) as eluent to give yellow powder. Yield: 41%. ^{1}H NMR (600 MHz, $CDCl_3$, ppm): 7.82-7.74 (m, 12H), 7.53-7.48 (m, 4H), 7.46-7.37 (m, 24H), 7.10-7.08 (d, 2H, J = 5.4 Hz), 7.06-7.04 (d, 2H, J = 5.4 Hz), 5.95 (s, 2H). ^{31}P NMR (243 MHz, $CDCl_3$, ppm): 18.6 (s, 1P, J_{Pt-P} = 2624 Hz).

Table S1. Crystallographic Data of Complexes **1**·5CH_2Cl_2, **2**·4CH_2Cl_2 and **3**·8$CHCl_3$.

	1·5CH_2Cl_2	**2**·4CH_2Cl_2	**3**·8$CHCl_3$
empirical formula	$C_{119}H_{112}Au_2Cl_{10}F_6N_2O_6P_6PtS_2$	$C_{114}H_{106}Au_2Cl_8F_6N_2O_6P_6PtS_4$	$C_{114}H_{98}Au_2Cl_{24}F_6N_2O_6P_6PtS_6$
formula weight	2973.56	2900.68	3523.94
crystal system	Triclinic	Triclinic	Monoclinic
space group	$P\bar{1}$	$P\bar{1}$	$P2_1/n$
a (Å)	17.6188(12)	15.1545(3)	15.4306(3)
b (Å)	21.4619(15)	15.4046(3)	22.5884(5)
c (Å)	21.4844(14)	15.8278(3)	19.2667(4)
α (deg)	116.219(2)	113.413(1)	90
β (deg)	99.238(2)	115.969(1)	98.195(1)
γ (deg)	105.677(2)	95.620(1)	90
V (Å^3)	6638.3(8)	2878.04(10)	6646.9(2)
Z	2	1	2
F (000)	2940.0	1432.0	3456.0
ρ_{calcd} (g/cm^3)	1.488	1.674	1.761
μ (mm^{-1})	3.618	4.160	3.961
Radiation (λ, Å)	0.71073	0.71073	0.71073
temperature (K)	150	150	150
GOF	1.023	1.025	1.015
Data Completeness	0.984	0.981	0.988
R1 (F_o)[a]	0.0395(18966)	0.0329(9588)	0.0292(10747)
wR2 (F_o^2)[b]	0.1192(24168)	0.0883(10361)	0.072(12067)

[a] $R1 = \Sigma|F_o - F_c|/\Sigma F_o$, [b] $wR2 = \Sigma[w(F_o^2 - F_c^2)^2]/\Sigma[w(F_o)^2)]^{1/2}$

Table S2. The Partial Molecular Orbital Compositions (%) by SCPA Approach in the Ground State and the Absorption Transitions for Complex **1** in CH_2Cl_2 Calculated by TD-DFT Method at the PBE1PBE-GD3 Level.

orbital	energy	MO contribution (%)			
	(eV)	Pt (s/p/d)	Au (s/p/d)	dTolmp	C≡C-TPA
LUMO+8	-1.16	8.45 (0/66/34)	8.77 (26/58/16)	46.38	36.40
LUMO+7	-1.29	2.70 (0/83/17)	7.13 (26/53/21)	83.52	6.65
LUMO+4	-1.41	1.71 (0/49/51)	14.05 (60/31/9)	82.61	1.63
LUMO+3	-1.50	7.31 (0/82/18)	8.57 (41/47/12)	83.11	1.01
LUMO	-2.41	12.07 (0/96/4)	18.41 (48/42/10)	63.44	6.09
HOMO	-5.47	5.33 (0/6/94)	0.40 (37/34/29)	2.52	91.76
HOMO-1	-5.62	1.24 (0/27/72)	0.84 (48/32/20)	3.63	94.29
HOMO-2	-6.62	35.15 (24/0/76)	38.49 (41/9/50)	24.70	1.67
HOMO-3	-6.72	18.90 (0/2/98)	1.00 (37/25/38)	5.97	74.13
HOMO-4	-6.88	25.41 (0/3/97)	1.78 (75/6/19)	14.20	58.60

state	*E*, nm (eV)	O.S.	transition (contrib.)	assignment	measured (nm)
S_1	499 (2.49)	0.2536	HOMO→LUMO (96%)	^{1}LLCT/^{1}LMCT	473
S_3	384 (3.23)	0.6407	HOMO-2→LUMO (97%)	^{1}MLCT/^{1}MC/^{1}IL	395
S_8	351 (3.53)	0.4179	HOMO-4→LUMO (49%)	^{1}LLCT/^{1}MC/^{1}IL	
			HOMO→LUMO+4 (27%)	^{1}LLCT/^{1}LMCT	
S_{12}	342 (3.62)	0.6794	HOMO→LUMO+7 (32%)	^{1}LLCT	345
			HOMO-1→LUMO+3 (27%)	^{1}LLCT/^{1}LMCT	
			HOMO→LUMO+8 (9%)	^{1}LLCT/^{1}IL/^{1}LMCT	
S_{15}	334 (3.71)	0.6064	HOMO-1→LUMO+3 (47%)	^{1}LLCT/^{1}LMCT	
			HOMO→LUMO+8 (24%)	^{1}LLCT/^{1}IL/^{1}LMCT	
			HOMO-1→LUMO+8 (9%)	^{1}LLCT/^{1}IL/^{1}LMCT	

Table S3. The Partial Molecular Orbital Compositions (%) by SCPA Approach in the Lowest-Energy Triplet State and the Emission Transitions for Complex **1** in CH_2Cl_2 Calculated by TD-DFT Method at the PBE1PBE-GD3 Level.

orbital	energy (eV)	MO Ccontribution (%)			
		Pt (s/p/d)	Au (s/p/d)	dTolmp	C≡C-TPA
LUMO	-2.67	12.48 (0/96/4)	22.49 (60/29/10)	58.74	6.30
HOMO	-5.40	5.64 (0/7/93)	0.45 (36/30/34)	2.50	91.41

state	*E*, nm (eV)	O.S.	transition (Contrib.)	assignment	measured (nm)
T_1	622 (1.99)	0.0000	HOMO→LUMO (83%)	^{3}LLCT/^{3}LMCT	609

Table S4. The Partial Molecular Orbital Compositions (%) by SCPA Approach in the Ground State and the Absorption Transitions for Complex **2** in CH_2Cl_2 Calculated by TD-DFT Method at the PBE1PBE-GD3 Level.

orbital	energy (eV)	MO contribution (%)			
		Pt (s/p/d)	Au (s/p/d)	dTolmp	C≡C-N,N-diphenylthiophen-2-amine
LUMO+18	-0.74	8.39 (69/11/21)	13.60 (69/26/5)	14.04	63.96
LUMO+17	-0.74	5.12 (26/67/7)	18.03 (56/39/5)	17.59	59.26
LUMO+13	-1.02	14.18 (2/98/0)	36.77 (91/7/2)	42.97	6.08
LUMO+4	-1.49	11.08 (0/100/0)	16.48 (22/67/11)	62.61	9.84
LUMO+2	-1.59	4.45 (10/78/12)	8.95 (15/70/15)	73.49	13.11
LUMO+1	-1.60	4.35 (33/19/48)	13.85 (24/70/6)	67.58	14.22
LUMO	-2.56	10.75 (0/100/0)	17.62 (45/41/13)	58.58	13.05
HOMO	-5.52	7.64 (20/0/80)	1.10 (56/24/19)	1.90	89.36
HOMO-1	-5.69	0.29 (0/97/1)	2.35 (60/11/28)	3.68	93.68
HOMO-2	-6.58	33.74 (32/0/68)	40.34 (42/12/46)	25.06	0.86

state	*E*, nm (eV)	O.S.	transition (contrib.)	assignment	measured (nm)
S_1	524 (2.36)	0.4468	HOMO→LUMO (97%)	^{1}LLCT/^{1}LMCT	490
S_3	383 (3.24)	0.654	HOMO-2→LUMO (97%)	^{1}MLCT/^{1}MC/^{1}IL	391
S_4	373 (3.33)	0.7108	HOMO→LUMO+2 (38%)	^{1}LLCT/^{1}IL	
			HOMO→LUMO+1 (22%)	^{1}LLCT/^{1}IL/^{1}LMCT	
S_7	358 (3.46)	0.1326	HOMO→LUMO+4 (60%)	^{1}LLCT/^{1}LMCT	356
			HOMO→LUMO+2 (19%)	^{1}LLCT/^{1}IL	
S_{28}	313 (3.96)	0.1452	HOMO→LUMO+13 (45%)	^{1}LLCT/^{1}LMCT	
			HOMO→LUMO+17 (14%)	^{1}IL/^{1}LLCT/^{1}LMCT	
			HOMO-1→LUMO+18 (10%)	^{1}IL/^{1}LMCT/^{1}LLCT	
S_{30}	305 (4.06)	0.1741	HOMO→LUMO+13 (33%)	^{1}LLCT/^{1}LMCT	
			HOMO→LUMO+17 (22%)	^{1}IL/^{1}LLCT/^{1}LMCT	
			HOMO-1→LUMO+18 (13%)	^{1}IL/^{1}LMCT/^{1}LLCT	

Table S5. The Partial Molecular Orbital Compositions (%) by SCPA Approach in the Lowest-Energy Triplet State and the Emission Transitions for Complex **2** in CH_2Cl_2 Calculated by TD-DFT Method at the PBE1PBE-GD3 Level.

orbital	energy (eV)	MO contribution (%)			
		Pt (s/p/d)	Au (s/p/d)	dTolmp	C≡C-N,N-diphenylthiophen-2-amine
LUMO	-2.73	13.41 (0/100/0)	25.46 (62/26/12)	51.37	9.76
HOMO	-5.21	10.66 (36/0/64)	2.05 (42/41/17)	3.40	83.89

state	*E*, nm (eV)	O.S.	transition (Contrib.)	assignment	measured (nm)
T_1	657 (1.89)	0.0000	HOMO→LUMO (85%)	^{3}LLCT/^{3}LMCT	640

Table S6. The Partial Molecular Orbital Compositions (%) by SCPA Approach in the Ground State and the Absorption Transitions for Complex **3** in CH_2Cl_2 Calculated by TD-DFT Method at the PBE1PBE-GD3 Level.

orbital	energy (eV)	MO Contribution (%)			
		Pt (s/p/d)	Au (s/p/d)	dTolmp	C≡C-4-phenyl-4H-dithieno-(3,2-b:2',3'-d)pyrrole
LUMO+9	-1.27	4.25 (0/100/0)	10.71 (36/32/31)	83.04	2.00
LUMO+8	-1.30	13.13 (0/100/0)	11.27 (36/47/16)	53.68	21.92
LUMO+6	-1.44	5.35 (0/100/0)	8.80 (51/18/31)	69.71	16.14
LUMO+3	-1.55	14.08 (52/0/48)	10.82 (44/40/16)	67.03	8.07
LUMO+2	-1.64	4.69 (0/100/0)	24.18 (65/32/3)	67.51	3.62
LUMO+1	-1.64	7.82 (49/0/51)	14.50 (50/49/1)	60.88	16.80
LUMO	-2.57	10.61 (0/100/0)	16.73 (45/38/17)	57.64	15.01
HOMO	-5.55	10.15 (6/0/94)	0.91 (49/18/33)	1.94	86.99
HOMO-1	-5.84	1.35 (0/99/0)	4.75 (37/19/44)	5.72	88.18
HOMO-2	-6.29	0.90 (49/0/50)	0.49 (62/20/18)	1.62	96.98
HOMO-3	-6.29	1.07 (0/100/0)	1.23 (49/41/10)	1.02	96.67
HOMO-4	-6.58	33.16 (29/0/71)	39.98 (37/14/49)	25.97	0.89
HOMO-5	-7.18	32.89 (28/0/72)	1.90 (25/37/39)	14.69	50.52

state	*E*, nm (eV)	O.S.	transition (Contrib.)	assignment	measured (nm)
S_1	518 (2.39)	0.819	HOMO→LUMO (98%)	^{1}LLCT/^{1}LMCT	495
S_3	384 (3.23)	0.6264	HOMO-4→LUMO (96%)	^{1}MLCT/^{1}MC/^{1}IL	390
S_{11}	348 (3.57)	0.3466	HOMO→LUMO+6 (79%)	^{1}LLCT/^{1}IL/^{1}MC	359
S_{13}	339 (3.65)	0.3643	HOMO-1→LUMO+1 (31%)	^{1}LLCT/^{1}IL/^{1}LMCT	339
			HOMO→LUMO+8 (27%)	^{1}LLCT/^{1}IL/^{1}LMCT	
			HOMO→LUMO+9 (13%)	^{1}LLCT/^{1}MC	
			HOMO-5→LUMO (10%)	^{1}LLCT/^{1}MC/^{1}IL	
S_{30}	302 (4.11)	0.2425	HOMO-3→LUMO+1 (45%)	^{1}LLCT/^{1}LMCT/^{1}IL	309
			HOMO-2→LUMO+2 (15%)	^{1}LLCT/^{1}LMCT	

Table S7. The Partial Molecular Orbital Compositions (%) by SCPA Approach in the Lowest-Energy Triplet State and the Emission Transitions for Complex **3** in CH_2Cl_2 Calculated by TD-DFT Method at the PBE1PBE-GD3 Level.

orbital	energy (eV)	MO contribution (%)			
		Pt (s/p/d)	Au (s/p/d)	dTolmp	C≡C-4-phenyl-4H-dithieno-(3,2-b:2',3'-d)pyrrole
LUMO	-2.76	12.28 (0/100/0)	17.92 (52/31/17)	54.58	15.22
HOMO	-5.39	10.45 (5/0/95)	0.94 (39/26/34)	1.85	86.76

state	*E*, nm (eV)	O.S.	transition (contrib.)	assignment	measured (nm)
T_1	652 (1.90)	0.0000	HOMO→LUMO (77%)	^{3}LLCT/^{3}LMCT	634

Table S8. The Optimization Procedures of the Devices Based on $PtAu_2$ Complex **1** by Modifying Doping Ratios, Host Materials and ETL Thickness.[a]

doping ratio	host material	thickness of ETL[b] (nm)	L_{max} (cd m^{-2})	V_{on} (V)	CE_{max} (cd A^{-1})	PE_{max} (lm W^{-1})	EQE_{max} (%)
5%	mCP:OXD-7 (1:1)	40	4719	5.0	17.2	8.7	5.2
5%	TCTA:OXD-7 (1:1)	40	12365	3.5	24.5	13.8	7.4
5%	TCTA:OXD-7 (1:1)	45	12121	4.4	37.4	15.0	11.4
5%	TCTA:OXD-7 (1:1)	50	10198	3.2	54.3	39.7	16.5
3%	TCTA:OXD-7 (1:1)	50	13407	3.4	48.5	31.7	14.7
8%	TCTA:OXD-7 (1:1)	50	12021	3.4	45.2	32.4	13.7

[a] Device structure: ITO / PEDOT : PSS (40 nm) / Poly-TPD (50 nm) / host materials : $PtAu_2$ complex (50 nm) / BmPyPb / LiF (1 nm) / Al (100 nm). [b] ETL = electron transport layer.

Table S9. The UV-Vis Absorption and Emission Data of Mononuclear Pt(II) Precursors **Pt-1**, **Pt-2** and **Pt-3** in CH_2Cl_2 solutions.

	λ_{abs} /nm (ε / dm^3 mol^{-1} cm^{-1})[a]	λ_{em} (nm)/ τ(ns) / Φ (%)
Pt-1	277(43700), 288(44700), 381(52700)	431 / 0.96 / < 0.5
Pt-2	297(22800), 393(27800)	572 / 2.1 μs / < 0.5 463 / 1.5 / < 0.5
Pt-3	325(51600), 413(87400)	596 / 2.6 μs / < 0.5 432 / 0.69 / < 0.5

[a] Measured at a concentration of 1×10^{-5} M.

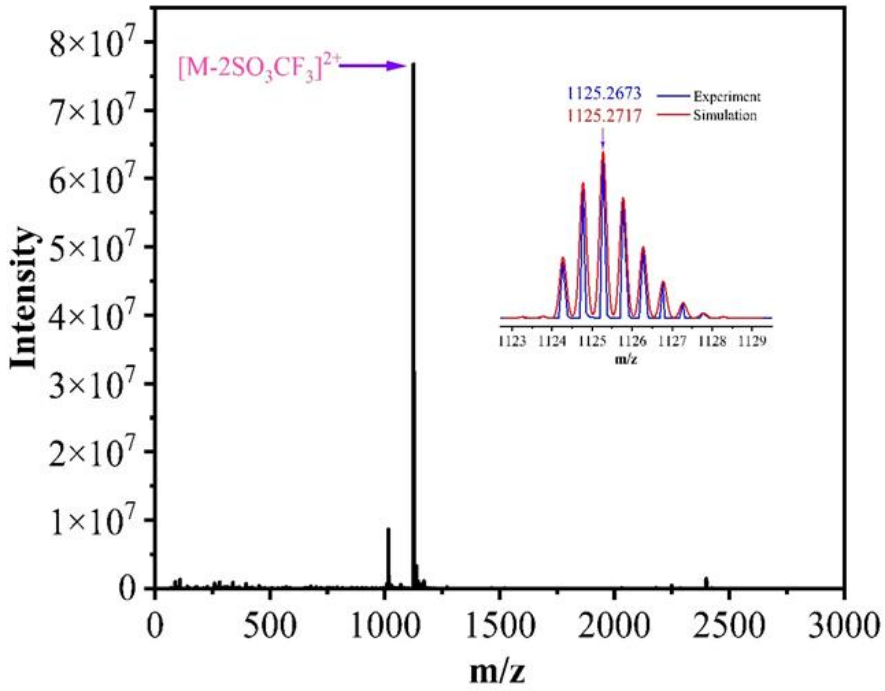

Fig. S1 The high-resolution mass spectrometry of complex **1**. Inset: The measured and simulated isotopic patterns.

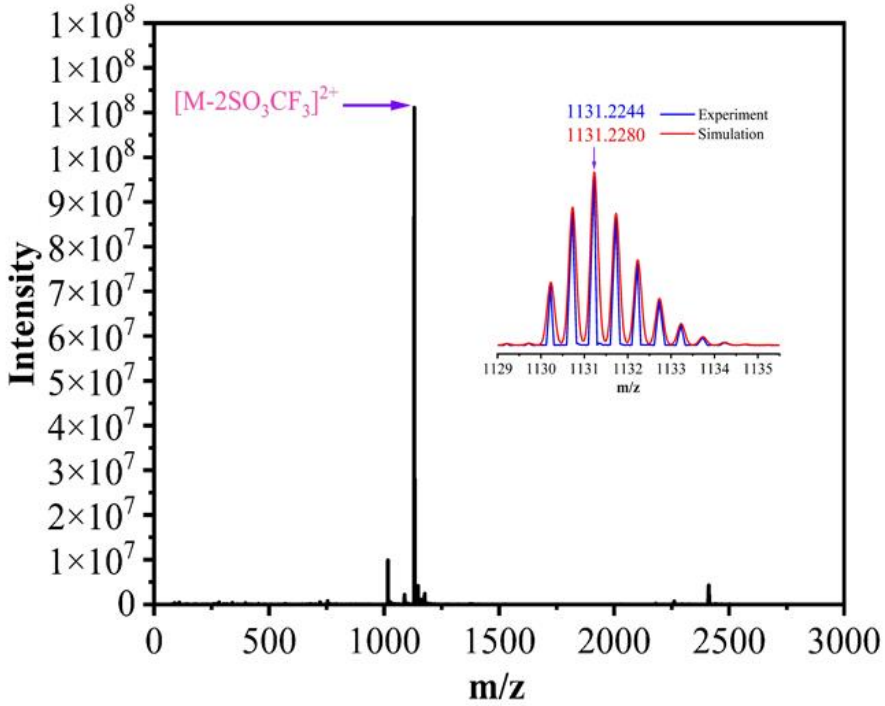

Fig. S2 The high-resolution mass spectrometry of complex **2**. Inset: The measured and simulated isotopic patterns.

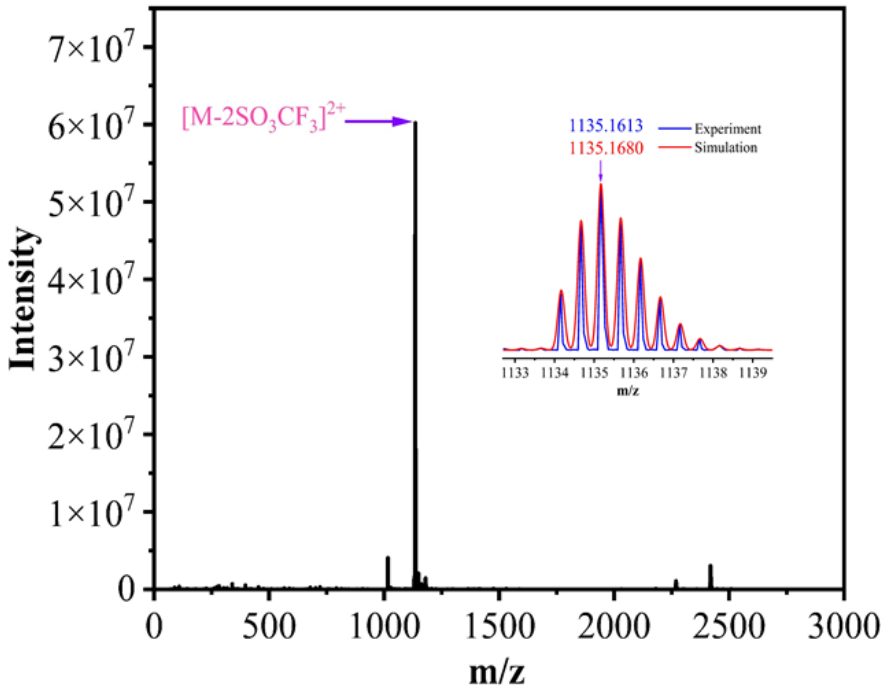

Fig. S3 The high-resolution mass spectrometry of complex **3**. Inset: The measured and simulated isotopic patterns.

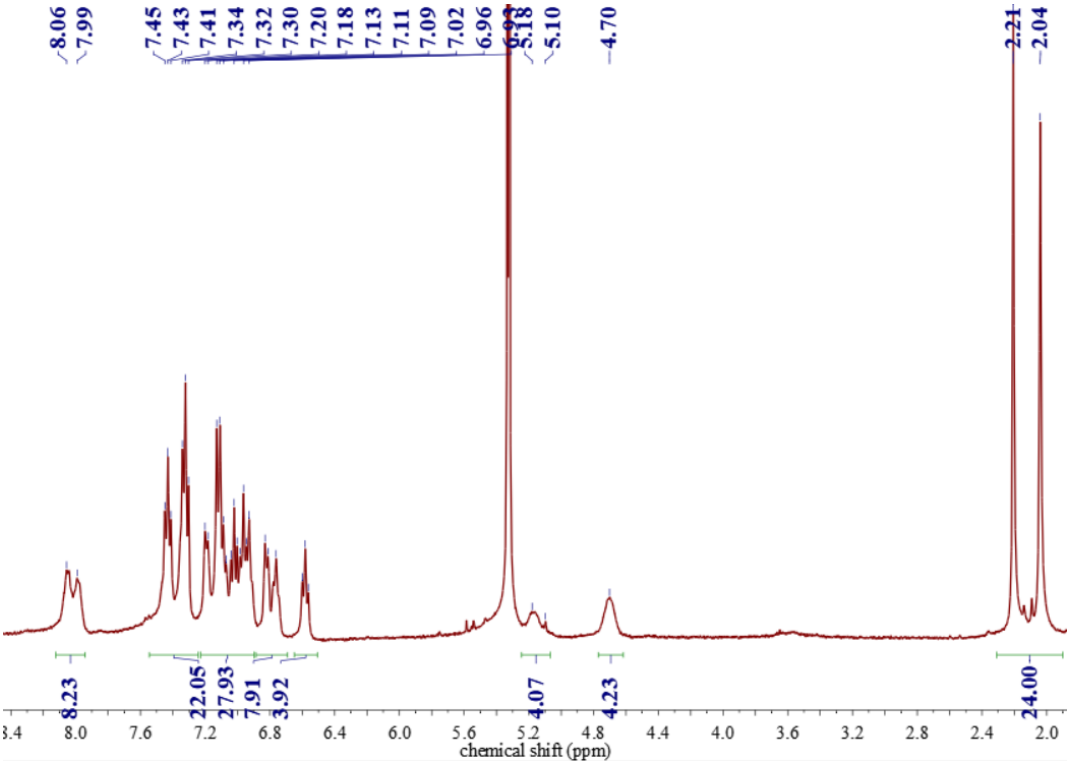

Fig. S4 The ^{1}H NMR spectrum of complex **1** in CD_2Cl_2 solution at ambient temperature.

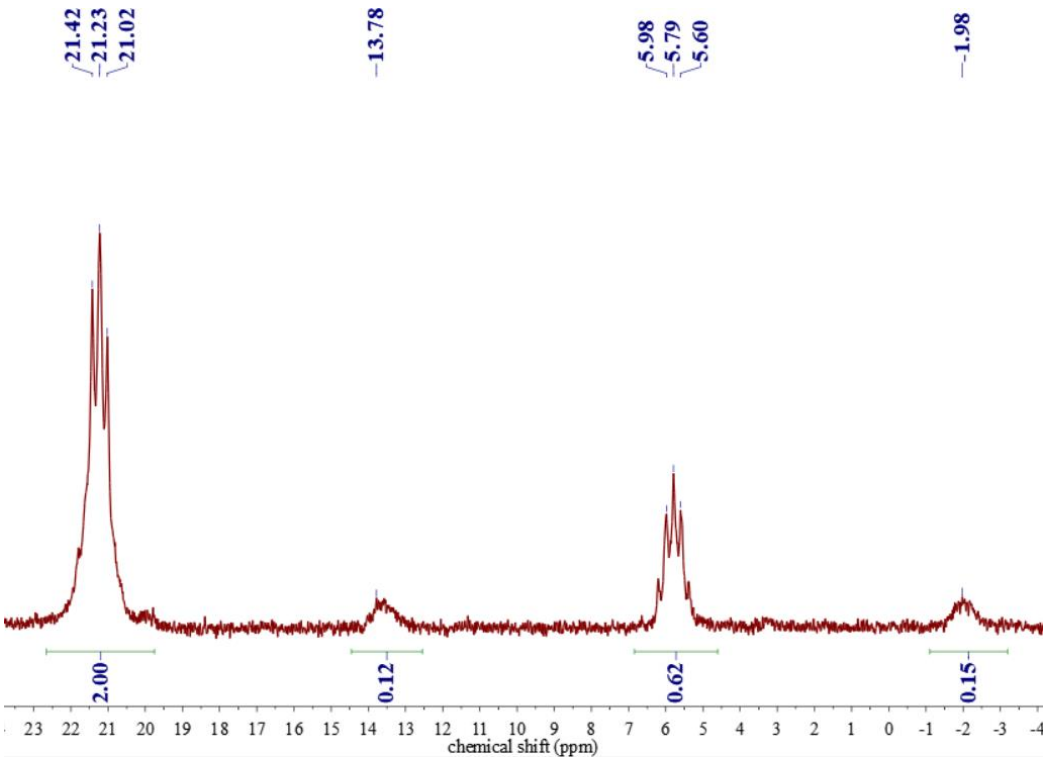

Fig. S5 The ^{31}P NMR spectrum of complex **1** in CD_2Cl_2 solution at ambient temperature.

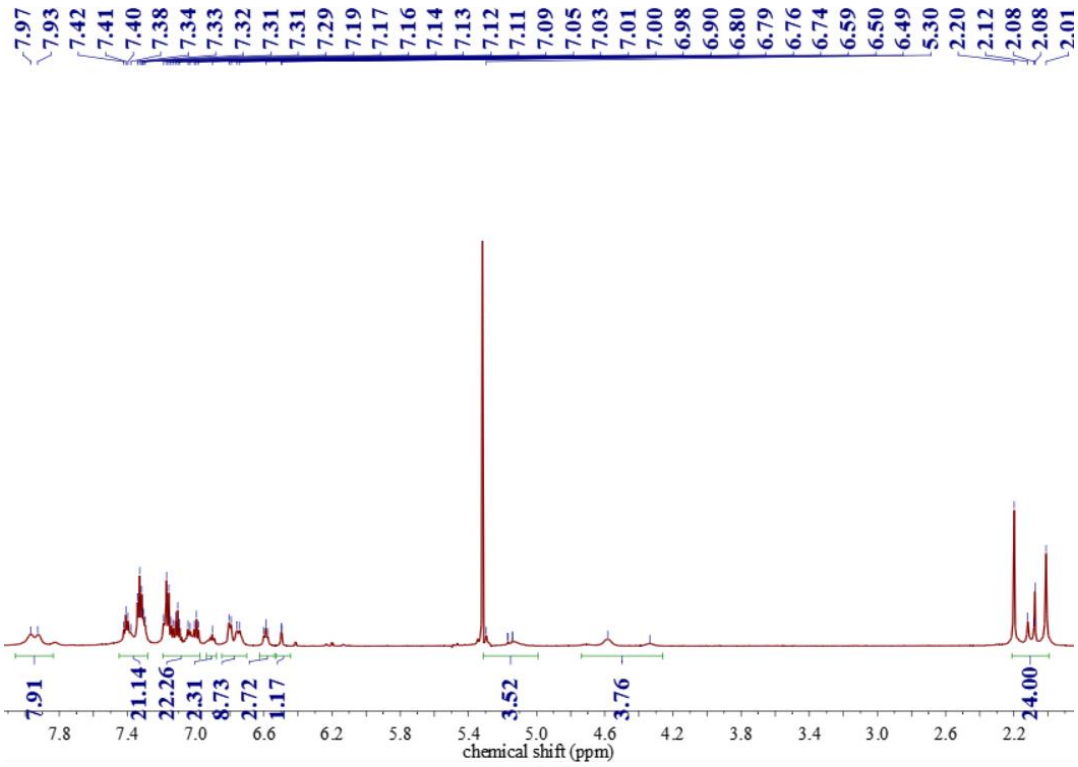

Fig. S6 The ^{1}H NMR spectrum of complex **2** in CD_2Cl_2 solution at ambient temperature.

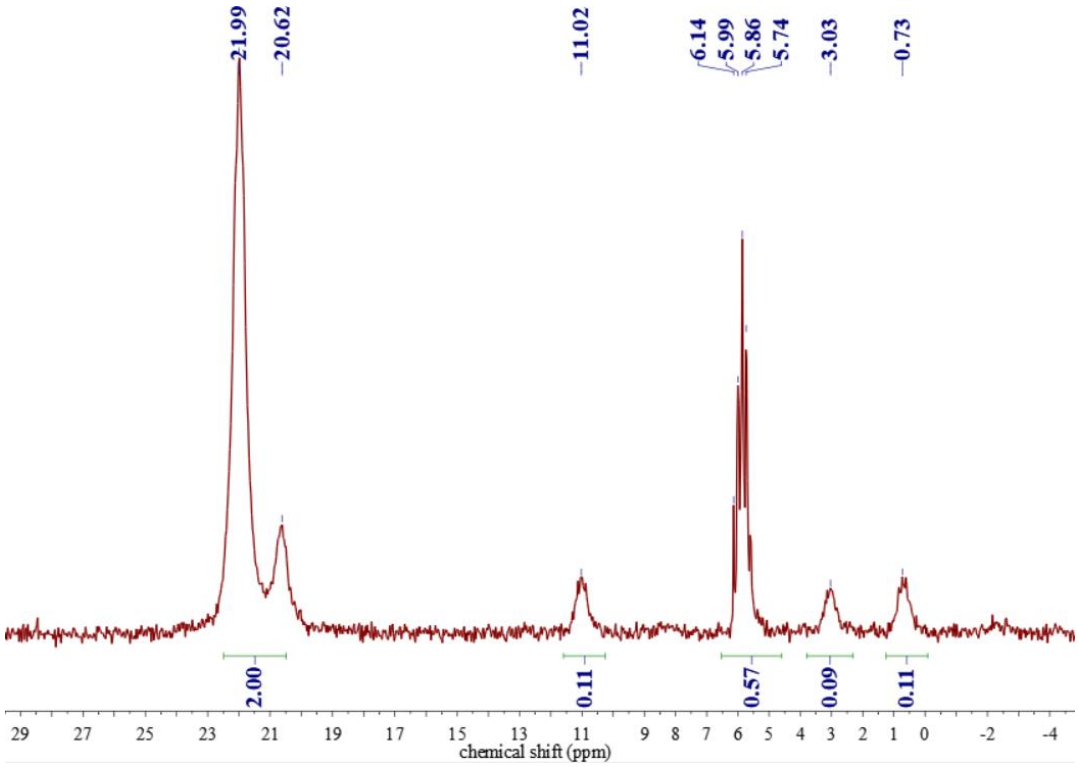

Fig. S7 The ^{31}P NMR spectrum of complex **2** in CD_2Cl_2 solution at ambient temperature.

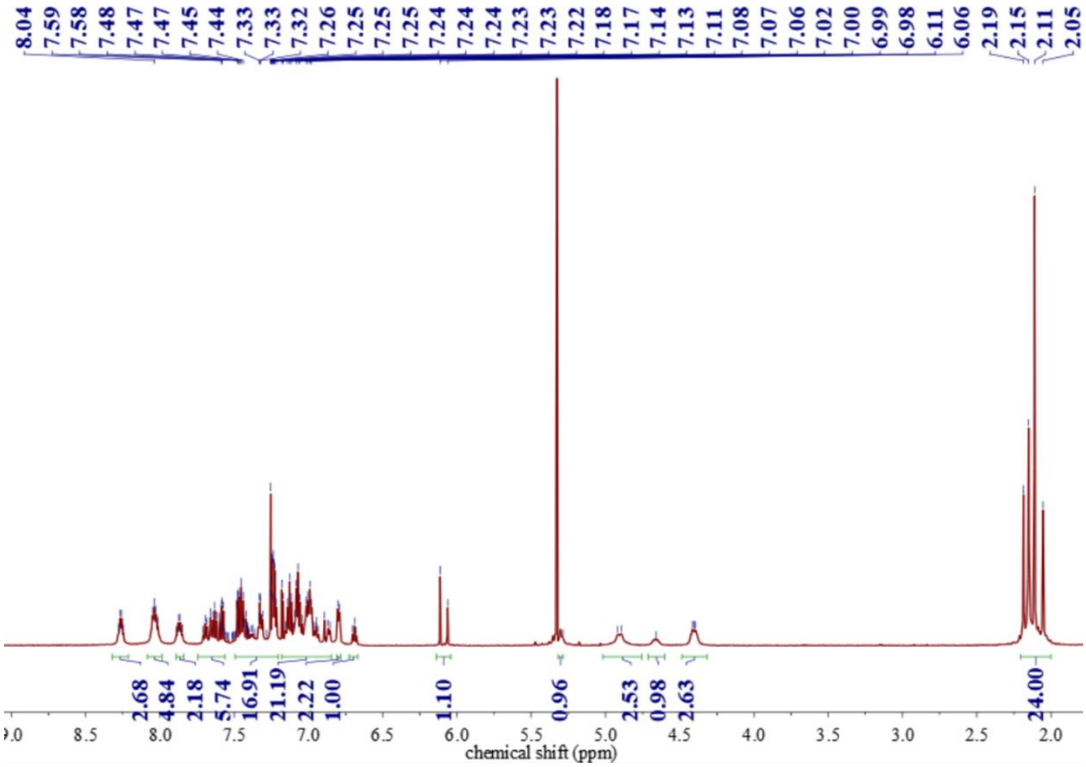

Fig. S8 The ^{1}H NMR spectrum of complex **3** in CD_2Cl_2 solution at ambient temperature.

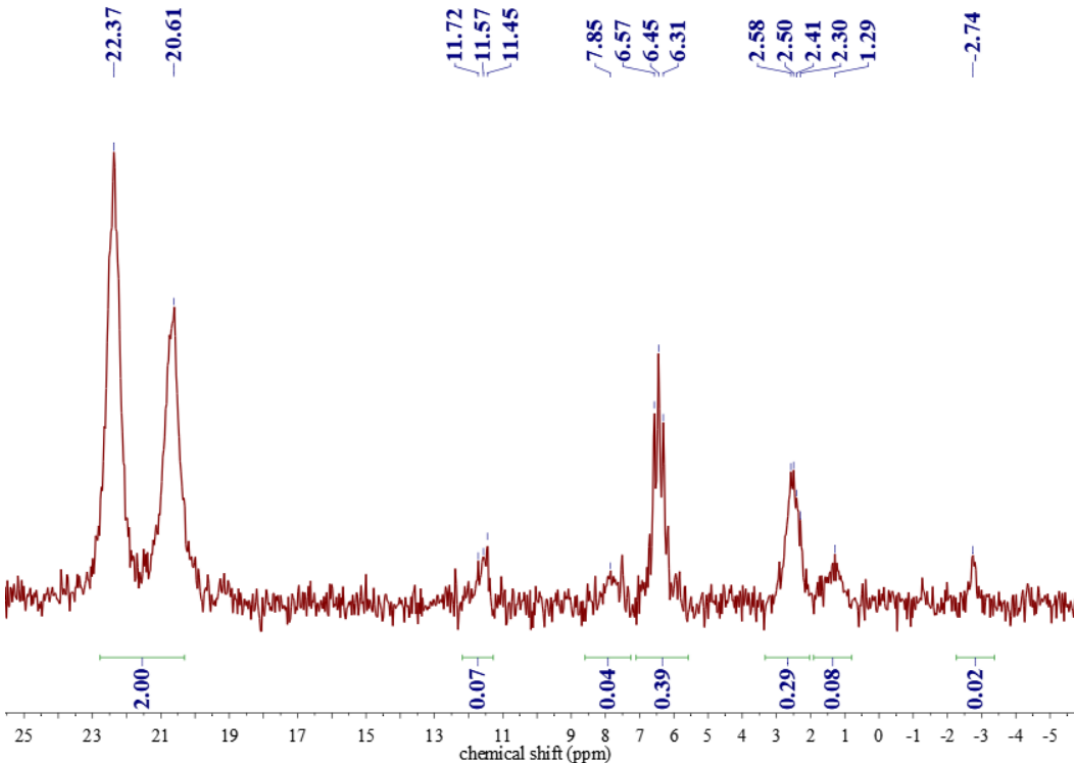

Fig. S9 The ^{31}P NMR spectrum of complex **3** in CD_2Cl_2 solution at ambient temperature.

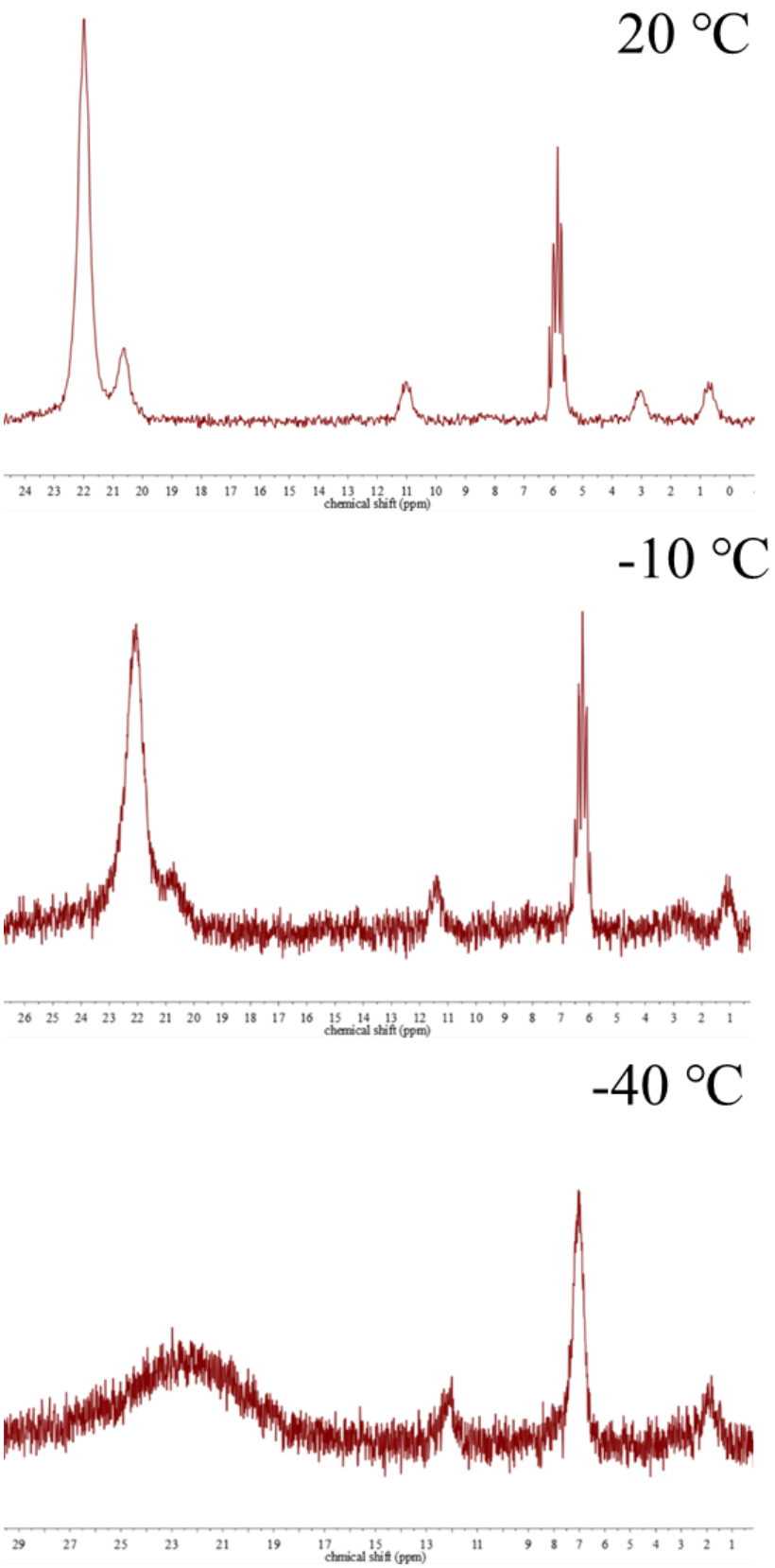

Fig. S10 The ^{31}P NMR spectra of complex **2** in CD_2Cl_2 solution at 20, −10 and −40 ℃.

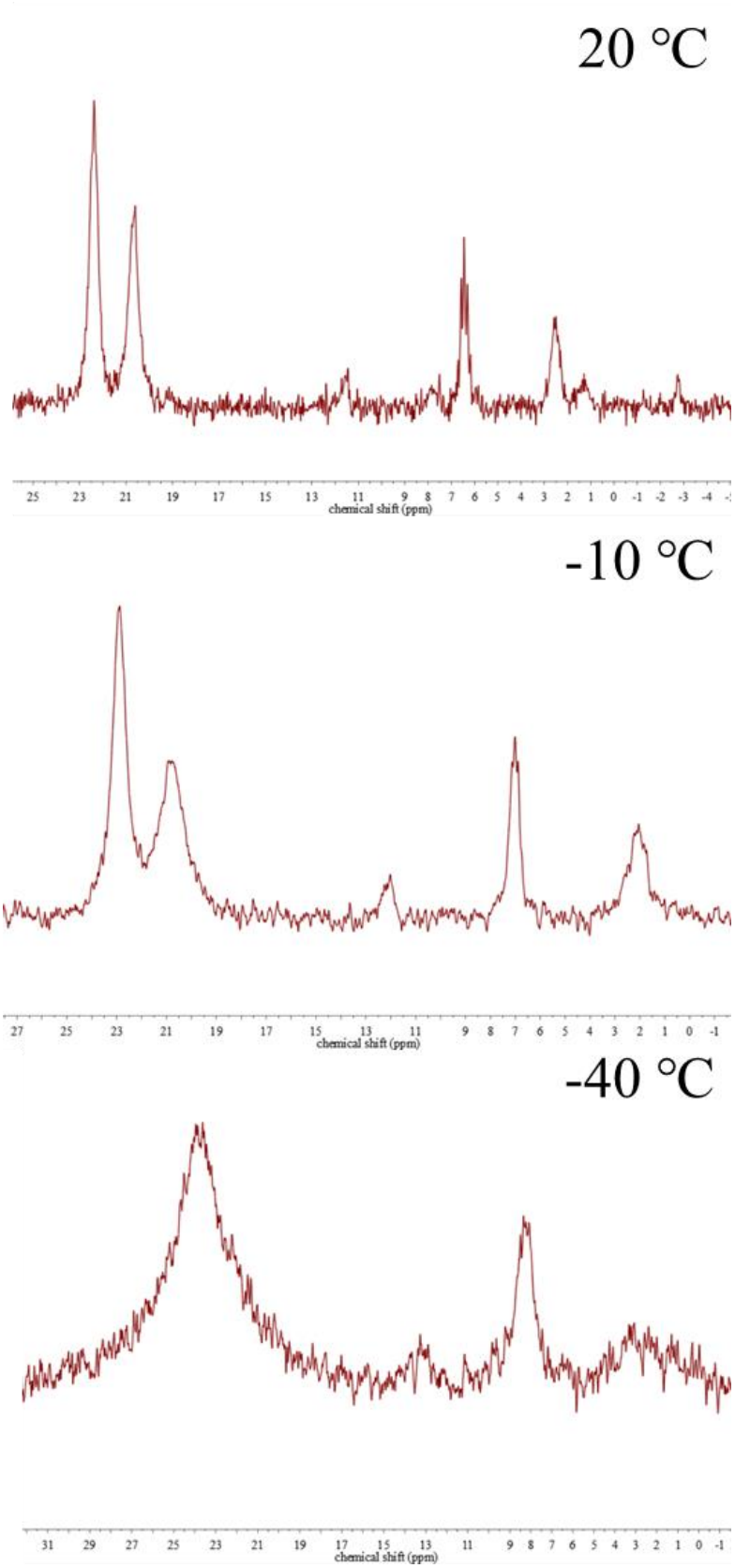

Fig. S11 The ^{31}P NMR spectra of complex **3** in CD_2Cl_2 solution at 20, –10 and –40 ℃.

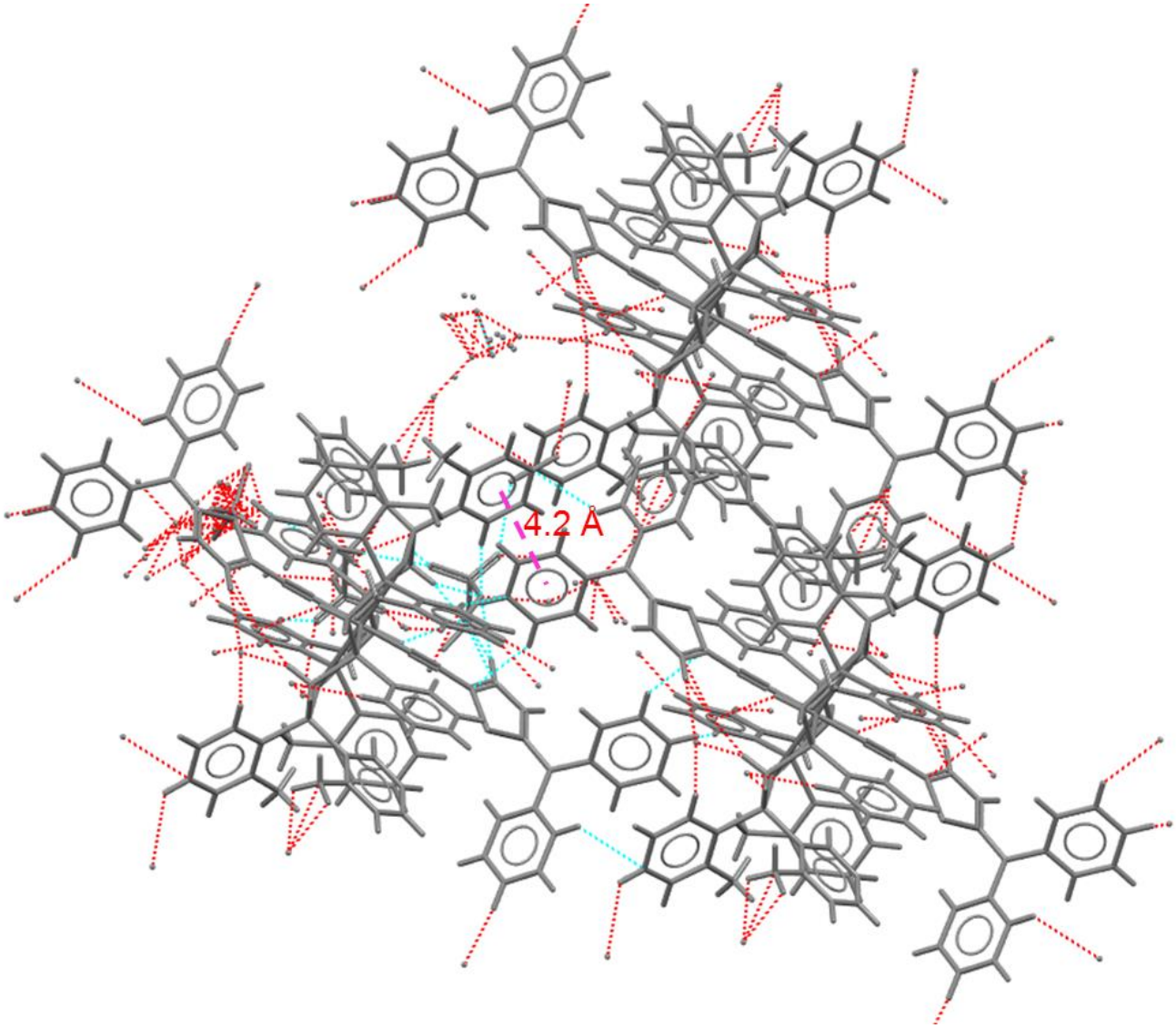

Fig. S12 The packing diagram of complex **2**, showing π-π stacking between phenyl rings and C-H···O hydrogen bonds between phenyl/thiophene C-H and trifluoromethanesulfonate O atoms.

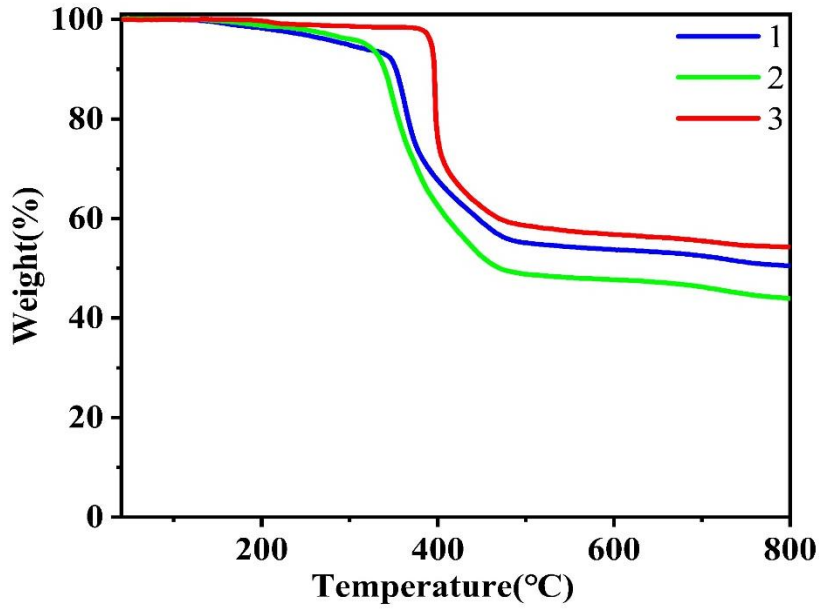

Fig. S13 The polts of thermogravimetric analyses of $PtAu_2$ complexes **1–3**.

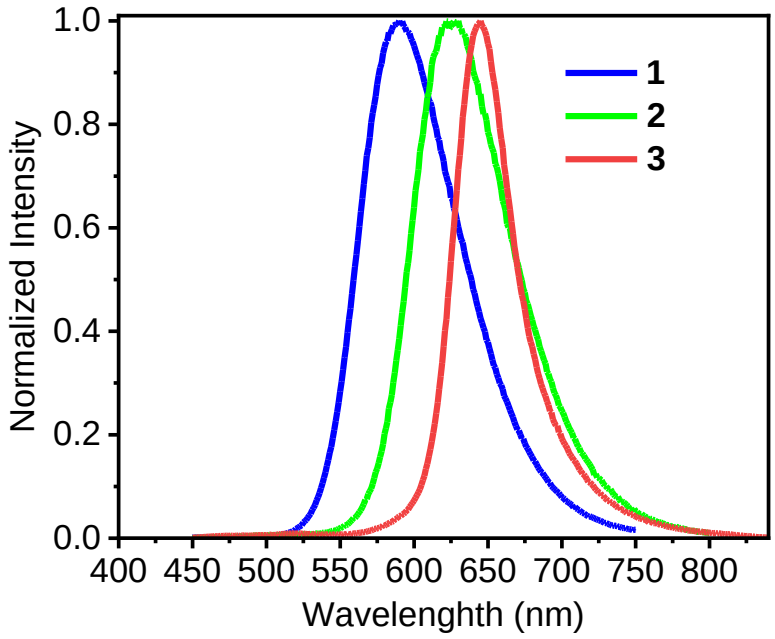

Fig. S14 The emission spectra of complexes **1–3** in solid state.

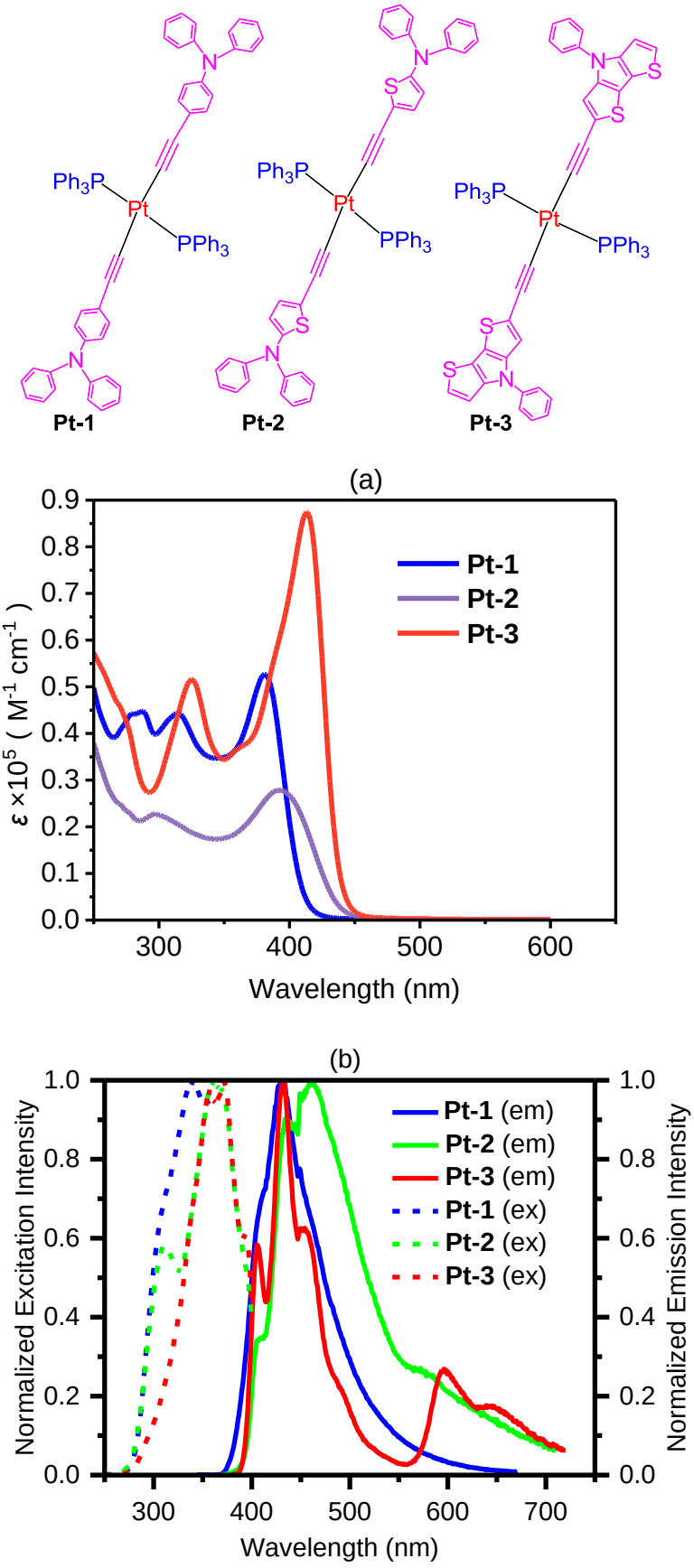

Fig. S15 The UV-Vis absorption spectra (a) together with excitation and emission (b) spectra of mononuclear platinum(II) precursors **Pt-1**, **Pt-2** and **Pt-3** in CH_2Cl_2 solutions at ambient temperature.

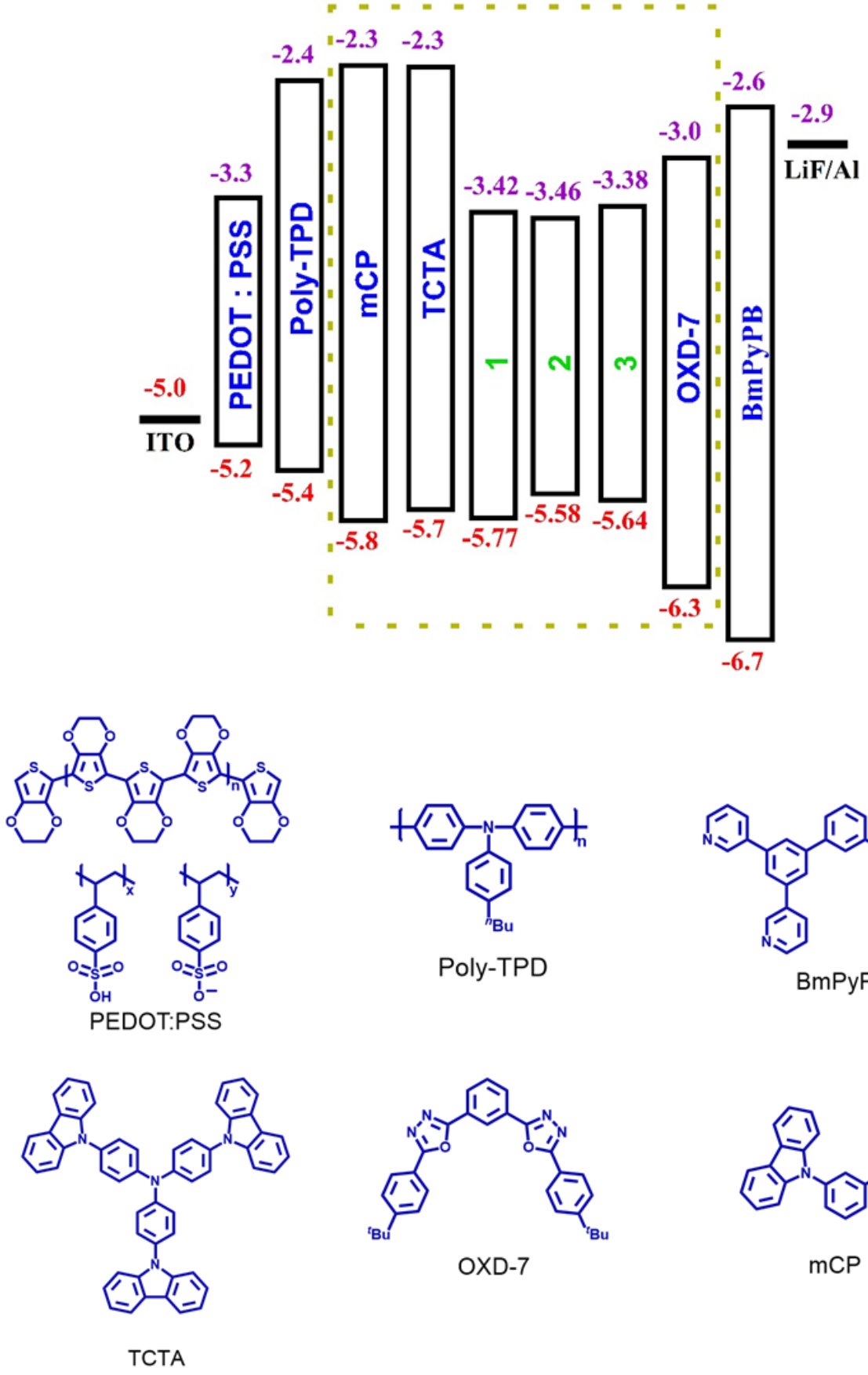

Fig. S16 Energy level diagrams in devices together with chemical structures of the materials used in OLEDs.

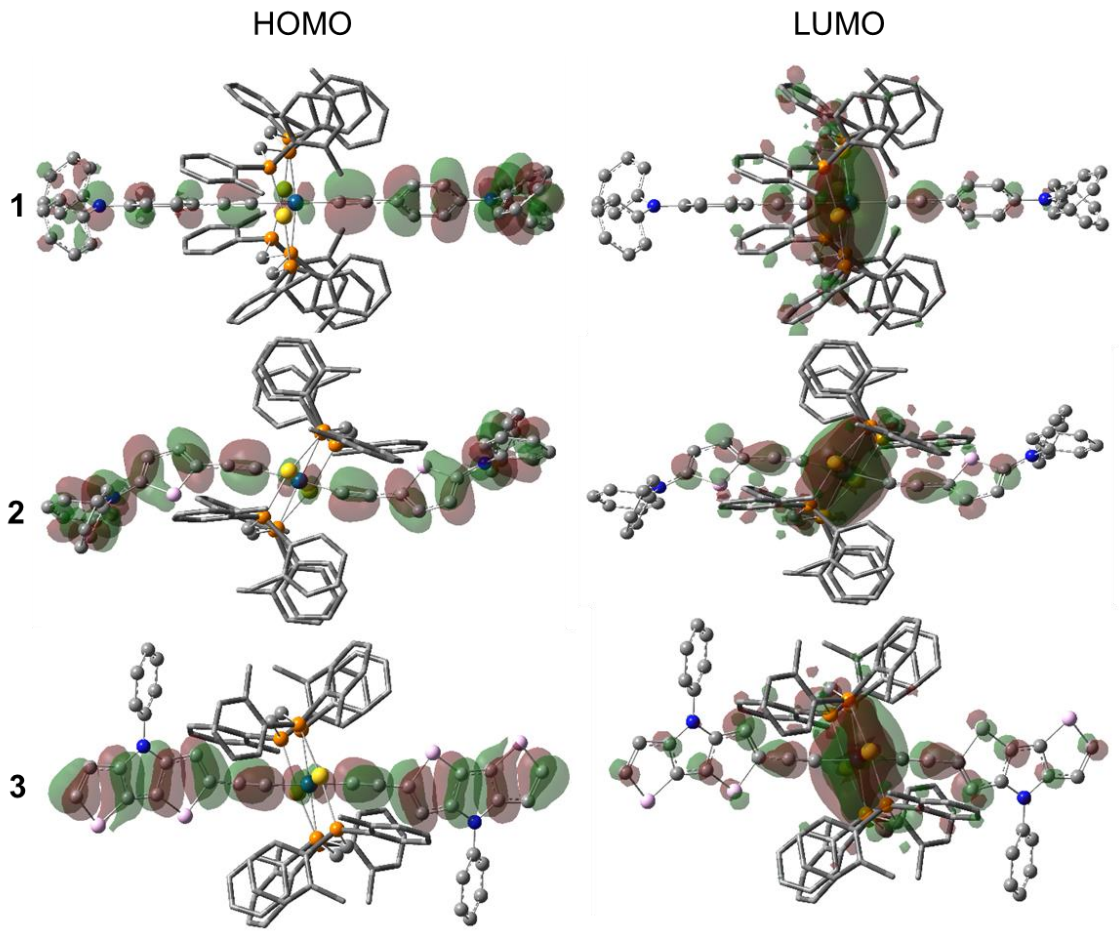

Fig. S17 Plots of the HOMO and LUMO involved in the absorption transition (isovalue = 0.02) for complexes **1–3** by TD-DFT method at the PBE1PBE-GD3 level.